B. Rauschenbach

Zentralinstitut für Kernforschung
Rossendorf
Akademie der Wissenschaften der DDR
8051 Dresden, Postfach 19, DDR

FORMATION OF COMPOUNDS BY HIGH-FLUENCE HITROGEN ION IMPLANTATION IN IRON AND TITANIUM

1. Introduction

In recent years it has been demonstrated that surface modification by high fluence implantation of metalloid ions can produce remarkable changes in the properties of metals. This technique has been applied to various metallic targets in order to improve their mechanical properties such as wear, fatique, friction /see for example ref. 1/.
Consequently, basic investigations of ion implantation metallurgy are essential so that this technique can be used effectively.
The object of this paper is to give an overview of our results on the field of implantation metallurgy of iron and titanium after nitrogen ion implantation.
So for only a few papers are known which have analysed the phases after nitrogen ion implantation in iron /2/ or titanium /3/.

2. Experimental conditions

The polycrystalline layers of iron or titanium were deposited on freshly cleaved NaCl or KCl, and on silicon in high vacuum of 10^{-3} Pa. Thickness of the layers was varied between 100 nm and 1 µm. The films were implanted at room temperature with nitrogen ions with energies from 30 to 60 keV in the dose range of $1 \cdot 10^{16}$ to $1{,}5 \cdot 10^{18}$ N^+-ions/cm^2. A lateral homogeneous distribution of nitrogen was obtained by wobbled nitrogen ion beam. The typical dose rate was 5 µA/cm^2. The choice of a low dose rate is important for a low heating of the specimens during implantation. The temperatures during implanta-

tion were kept below 50°C. Auger electron spectrometry /AES/ measurements were performed to analyse the implantation profiles and impurity contents /carbon, oxygen/ of unimplanted and implanted titanium targets. Measurements with the aid of the AES show that the accuracy of ion dose was better than 92 %. The crystallographic structure and morphology of the titanium layers before and after implantation were investigated by high-voltage electron microscopy /HVEM/ and transmission high-energy electron difftraction /THEED/. Studies were made by the use of the 1 MeV electron microscope JEM-1000 and selected area diffraction /SAD/ technique.
A problem at high voltages / 300 ... 500 keV/ are knock-on displacement damages. Our experiments shown that these dagages are negligible under our operating conditions /small electron fluxs, low temperatures/.
Identification of phases after implantation took place on the basis of electron scattering diffractions diagrams. The electron scattering curves were obtained by calibrated selected area diffraction patterns. Salibration of SAD-patterns is generally straightforward but can be facilitatet by using an internal standard /unimplanted region/ since the camera constant in the electron microscope is sensitive to change in specimen position.
It is known that implantation of metalloid ions lead to formation of many various phases. Electron diffraction reflections of these phases are overlapped partially. Therefore it is a great problem to determine positions and intensities of these peaks. Two computer programs are used to calculate the interplanar spacings, intensities and synthetic electron diffraction spectrums.
First, a method is used to calculate positions and intensities of separately electron diffraction reflections. This technique involves the fitting equidistantly spaced data to a quartic equation and determination of different derivations of the electron diffraction spectrum /details see ref. /4//.

Second, the electron diffraction spectrum is converted into digital data. These segments are fitted with interpolating cubic spline functions /details see appendix/.

3. Results and discussion

3.1. Distribution of nitrogen in iron and titanium

Fig. 1 shown the concentration of nitrogen and carbon in titanium after an implantation of $1 \cdot 10^{18}$ N^+-ions/cm^2. Fig. 2 shows data typical of iron implanted to $1 \cdot 10^{17}$, $5 \cdot 10^{17}$ and $1 \cdot 10^{18}$ N^+-ions/cm^2. The determined concentration distributions are shallower than those preticted by the LSS-theory and the concentration profiles show a deeper penetration of implanted nitrogen. Also the nearsurface region contains a higher nitrogen concentration. The nitrogen distribution shows a plateau region in the centre of the distribution. Generally, the concentration distribution of implanted metalloid ions with doses $1 \cdot 10^{17}$ ions/cm^2 is very different from the nitrogen distribution preticted by the LSS-Theory /5/. Dominant roles in modification of concentration profiles are possibly played by phenomena like sputtering /preferential sputtering/, solid solubility limits, diffusion /thermal and radiation-enhanced diffusion/, phase formation and transformation, and, in all probability, by the important effect of ion beam mixing /5,6,7/.
The cascade of collisions can give rise to the mixing of implanted and host atoms because both types of atom can become recolated. The cascade mixing mechanism is very efficient because the significant majority of displacements of implanted atoms occur as a result of impacts of recoiling atoms. Recently, we used the results of the ion beam mixing theories /8,9/ for calculating the broadening and shift of the concentration profiles. For example, Fig. 1 shows a comparison of the concentration distribution of nitrogen in titanium with consideration of sputtering, broadening, and shift /solid line/. In view of the fact that our calculations are a rough approxima-

tion, the agreement is good. The concentration distributions exhibit a shift to higher depth and great broadening /plateau/ as a function of ion fluences. The influence of mixing is low at doses = $1 \cdot 10^{17}$ N^+ ions/cm^2. The concentration in the near-surface region is smaller than the experimentally measured concentration. Likely, this is the reason for radiation-enhanced diffusion via mobile vacancies.

3.2. Nitrogen ion implantation in titanium

Fig. 3 shows a selected area diffraction pattern /SAD/, the bright field /BF/ and dark field /DF/ of titanium implanted with $5 \cdot 10^{17}$ N^+-ions/cm^2. In order to identify the phases of implanted layer, the approach was used which is demonstrated in /4/ and in appendix. Beside these phases other titanium modification and compounds were checked. The allotropic modification of titanium, the high-temperature form -Ti /fcc/ and high-pressure form -Ti /hex/, and various titanium oxydes, the triclinic structure Ti_nO_{2n-1} /Ti_7O_{13}, Ti_8O_{15}, Ti_9O_{17}/, anatase /tetrag./ and brookite /orthorhomb./, could not be identified.
Debeye-Scherrer rings of -titanium could be identified in all analysed THEED pattern, The dark precipitations of Fig.3 /bright field/ could be proved as the cubic face-centred titanium nitride phase -TiN_x. This phase can be identified in the dose range from $1 \cdot 10^{16}$ to $5{,}5 \cdot 10^{8}$ N^+-ions/cm^2. The dark field mode is especially useful in determing the size, distribution and morphology of precipitates /10/.
It should be noted that the -TiN_x precipitations produced by high-fluence nitrogen ion implantation / $5 \cdot 10^{17}$ N^+ - ions/cm^2/ have a preferential orientation. With aid of a special goniometer equipment in the HVEM, it was possible to determine mictroscopical inhomogenities of texture. It was been found a fibre arrangement of these nitrides. Exact calculations are prepared on base of incomplete pole figures /10,11/.

At implantation dose above 1 . 10^{17} ... 2,5 . 10^{17} N^+-ions/ /cm^2 reflections from the tetragonal -Ti_2N phase start to appear beside the -TiN_x phase. This phase is present only in a narrow composition range about 33 ar.-%. The -Ti_2N phase could be found after nitrogen ion implantation into -titanium at room temperature in the dose range between 1 . 10^{17} ... 2,5 . 10^{17} N^+-ions/cm^2 and 1,5 . 10^8 N^+-ions/ /cm^2. At high implantation doses /2,5 . 10^{17} ... 5 . 10^{17} N^+-inions/cm^2/ could by analysed not only titanium nitrides but also titanium carbonitrides and titanium carbides. Also different RHEED reflections, /101/, /200/, /120/ and /220/, of rutil TiO_2 /tetrag./ could be detected in any cases. A dependence of formation of rutil on implantation dose, temperature and vacuum conditions was not found. Because of carbon adsorption during the implantation process and recoil implantation by nitrogen ion bombardment the titanium layer is additionally doped with carbon. Measurements with the help of Auger electron spectroscopy /AES/ show that carbon is transported to a depth of 50 ... 80 nm at doses 1 . 10^{17} N^+-ions/cm^2. It is known, that carbon can occupy the lattice sites of nitrogen in metal carbonitride phases. Nitrogen ion implantation of titanium with high doses lead to formation of cubic TiC_yN_x and TiC_x. The structure of the titanium carbonitride phase is isomorph to the TiN_x phase. Nitrogen and carbon portions on octahedral places /interstitial/ of the face-centred cubic TiC_yN_x phase are depended on the implantation dose. It is impossible that the habit of -TiN_x and TiC_yN_x precipitations can be distinquished in bright or dark field of Fig. 3.

A pure titanium carbide phase could be proved after implantation of nitrogen ions with a dose 5 . 10^{17} N^+-ions/cm^2. On base of these investigations a "state diagram" or a diagram of existence range can be drawn /4,12/.

In Fig. 4 this diagram is represented. As opposed the equilibrium phase diagram at room temperature it includes metasta-

ble phases and partially opposes the Gibbs phase rule. Such state diagrams are known from systems boron/iron /13/ and niteogen/iron /14,15/. The cause of this behaviour must be sought in the thermodynamical non-equlibrium process of ion implantation. Results of nitrogen ion implantation induced titanium nitride formation agree well with the few published results /3/.

Recently, a model of implantation-inducent transition was proposed to explain phase transformation of iron after nitrogen ion implantation /see point 3.3/. This model can be also used for the explantation of phase formation of titanium after nitrogen ion implantation /12/.

3.3. Nitrogen ion implantation in iron

Fig. 5 shows a HVEM micrograph of iron implanted with $5 \cdot 10^{17} N^+$-ions/cm^2. Identification of phases after implantation take places by electron diffraction contrast /morphology implantations/, selected area diffraction /lattice structure analysis/ and comparison of the measured intersities with the calculated intensities of the diffraction reflections /14,15/. This figure demonstrates also the different habit of the implantation - induced phases. The type of the formed iron nitride phases is depended on the implantation dose.

- dose range $1 \cdot 10^{16}$ to $4 \cdot 10^{16}$ N^+-ions/cm^2

  In this dose range we found the -iron nitride solid solution only. Depending on the implantation dose the nitrogen portion on octahedral places of the f.c.c. austenite is varied /14/.

  Under conventional conditions of production this solid solution exist only above the eutectic point.

- dose range $4 \cdot 10^{16}$ to $1 \cdot 10^{18}$ N^+-ions/cm^2

  From about $4 \cdot 10^{16}$ N^+-ions/cm^2 other iron nitride phases appear to the -austenite additionally. The nitride phases -martensite, -$Fe_{16}N_2$ and of exclusively metastable constitution. The -nitride precipitations /b.c.t./ are

expected to be trapped as plates on the /100/ plane of -iron. The -iron nitride has a high technical importance because precipitations of this phase are responsible for the improvement of several mechanical properties /increased fatique lifetime /16/, decreased wear /17/.

is a phase with high nitrogen content. For example, while up to the implantation dose of $1 \cdot 10^{17}$ N^+-ions/cm^2 about 32 to 36 nitrogen atoms are inserted per hundred iron atoms, this portion increases with implantation dose to about 42 to 48 at-% nitrogen in -nitride after implantation of $1 \cdot 10^{18}$ N^+-ions/cm^2 /14/. Additionally to -$Fe_{16}N_2$ and -Fe_2N_{1-x}, -martensite. Numerous needle-shaped crystallites are formed at room temperature implantation /14/.

On the basis of these extensive investigations a "state diagram" can be drawn which reflects this assignment. In Fig. 6 the state diagram is represented. In difference to the equilibrium phase diagram includes metastables phases and partially opposes the Gibbs phase rule. The cause of this behaviour must be sought in the non-equilibrium process of ion implantation. In Fig. 6 the dependence of iron nitride phases on implantation dose and thermal treatment is represented phase transformation by thermal treatment are discussed in refs. /13/, /15/. Iron is additionally doped with carbon adsorption during the implantation process and recoil implantation by nitrogen ions. Different iron carbonitride and iron carbide could be found /18/.

Recently, a model of implantation-induced phase transition was proposed to explain phase transformation of iron after nitrogen ion implantation /15/. It is assumed that the penetrating of ions into a target initiate compression waves in the displacement cascade /spike/ which lead to extreme pressure pressures and temperatures for a very short time /10^{-10} ... 10^{-12} sec / /19,20/. Caused by the extreme spike life time such phases are formed which only require lattice

in variant deformation. According to this model an implantation of 30 ... 60 keV nitrogen ions in iron results in pressures to 100 ... 120 GPa and temperatures to 1000 ... 1500°C /20/. According to Bundy /21/ iron exhibits behind the -low temperature phase /b.c.c./ and the -high temperature phase /f.c.c./ a hexagonal -high pressure phase /Fig.7/. These iron modifications can be transformed by little lattice invariont deformation into ε-$Fe_{10}N_2$ /of type I/, -austenite, -martensite and ε-Fe_2N_{1-x}. By thermal treatment a diffusion determined process joines this deformation process /details see Fig. 7 and refs. /13,15/.

4. Appendix - Using of cubic spline functions for phase analysis

The electron diffraction spectrum in converted into digital segments. These segments are described with spline function, where x is the a position within the segment /x_k, x_{k-1}/ and I is the intersity at the point x after background separation. The technique of spline functions is demonstrated by Ahlberg et al. /2/ and Greville /23/.
Using a cubic polynom in the following form.

$$P_k\,/x/ = A_k\,/x - x_k/^3 + B_k\,/x-x_k/^2 + C_k\,/x-x_k/ + D_k \qquad /1/$$

where k=1 ... n.

The 4/n-1/ coefficient A_k, B_k, C_k and D_k must be determined, where the spline conditions /22,23/ must be accomplished. Within the interval /segment/, the values of the function, the first deriation and second derivation of splines at x_k and x_{k+1} given by

$$I_k = D_k \qquad /2a/$$

$$I_{k+1} = A_k \Delta x_k^3 + B_k \Delta x_k^2 + C_k \Delta x_k + D_k \qquad /2b/$$

$$I'_k = C_k \qquad /3a/$$

$$I'_{k+1} = 3A_k \Delta x_k^2 + 2B_k \Delta x_k + C_k \qquad /3b/$$

$$I''_k = 2B_k \qquad /4a/$$

$$I''_{k+1} = 6\,A_k\,\Delta x_k + 2\,B_k \qquad /4b/$$

where $\Delta x_k = x - x_k$

Additionally to Eq. /2a/ it is possible to calculate the coefficients on the baso of Eqs. /2b/ - /4b/.

$$A = \frac{1}{6\,\Delta x_k}\left(I''_{k+1} - I''_k\right) \qquad /5a/$$

$$B = \frac{1}{2}\,I''_k \qquad /5b/$$

$$C = \frac{\Delta I_k}{\Delta x_k} - \frac{1}{6}\,\Delta x_k\left(I''_{k+1} + 2\,I''_k\right) \qquad /5c/$$

The demand for steady

$$P'_{k-1}(x_k) = P'_k(x_k), \text{ where } k = 2, \ldots, n-1 \qquad /6/$$

leading to the conditions

$$3\,A_{k-1}\,\Delta x^2_{k-1} + 2\,B_{k-1}\,\Delta x_{k-1} + C_{k-1} = C_k \qquad /7/$$

or to n-2 equations for the unknown qualities I"

$$\Delta x_{k-1}\,I''_{k-1} + 2(\Delta x_{k-1} + \Delta x_k)\,I''_k + \Delta x_k\,I''_{k+1} = 6\left(\frac{\Delta I_k}{\Delta x_k} - \frac{\Delta I_{k-1}}{\Delta x_{k-1}}\right) \qquad /8/$$

where k = 2, ..., n-1/

On the base of Eqs. /5a-c/ and with the aid of the measured values I_k, m the coeffizient of /5a-c/ can be determined. If Y''_1 and Y''_n is given, then Eq. /8/ can given a quadric linear equation system by

$$\begin{bmatrix} 2(\Delta x_1 + \Delta x_2) & \Delta x_2 & & & \\ \Delta x_2 & \ddots & \ddots & & \\ & \ddots & \ddots & \Delta x_{n-2} & \\ & & \Delta x_{n-2} & 2(\Delta x_{n-2} + \Delta x_{n-1}) & \end{bmatrix} \begin{bmatrix} y_2'' \\ y_3'' \\ \vdots \\ y_{n-1}'' \end{bmatrix} = \begin{bmatrix} 6\left(\frac{\Delta y_2}{\Delta x_2} - \frac{\Delta y_1}{\Delta x_1}\right) - \Delta x_1 y_1'' \\ \vdots \\ 6\left(\frac{\Delta y_{n-1}}{\Delta x_{n-1}} - \frac{\Delta y_{n-2}}{\Delta x_{n-2}}\right) - \Delta x_{n-1} y_n'' \end{bmatrix}$$

for $y_2'', \ldots y_{n-1}''$

The equation system /9/ can be solved with the helb of the algorithm by GauB and Pivot-search.
By applying of this method it is possible to find positions of overlapped peaks and to compute a synthetic spectrum.

5. References

/1/ H.Herman, Nucl. Instr. Meth. 182/183 /1981/ 887
G.Rearnaley, Thin Solid Films 107 /1983/ 315
K.Hohmuth, E.Richter, B.Rauschenbach and C.Blochwitz, Mater. Sci. Eng. 69 /1985/ 191

/2/ G.Prinzipi, P.Matteazzi, R.Ramous and G.Longworth, J.Mater.Sci. Lett. 15 /1980/ 2665.
G.Longworth and N.E.W. Hartley, Thin Solid Films 48 /1978/ 95.
C.A. dos Santos, J.I.R. Baumvol, E.A. Garcia and M.Behar, J.Phys. D:Appl. Phys. 17 /1984/ 969

/3/ V.N. Bykov, V.A. Troyan, G.G.Zotorovtseva and V.S.Khaimovich, phys. stat. sol. /a/ 32 /1975/ 53.
M.Belii, F.F. Komarov, V.S. Tishkov and V.M.Yankovskii, phys. stat. sol. /a/ 45 /1978/ 343
P.A. Chen and T.T. Yang, Thin Solid Films 63 /1981/ L91
J.P. Gauthier, D.Eleche, J.Pivol and J.A.Roger, Vacuum 34 /1984/ 1013

/4/ B.Rauschenbach, J.Mater. Sci. 21 /1986/ No. 1

/5/ B.Rauschenbach, G.Blasek and R.Dietsch, phys. stat. sol. /a/ 85 /1984/ 473

/6/ H.Kräutle, Nucl. Instr. Meth. 134 /1976/ 167

/7/ A.Gras-Marti, J.J.Jinenez-Rodriguez, J.Peon-Fernandez and M.Rodriguez-Vidal, Phil. Mag. A 45 /1982/ 191

/8/ V.Lettmark and W.O. Hofer, Rep. Jül-1974, /1984/

/9/ P.Sigmund and A.Gras-Marti, Nucl. Instr. 182/183 /1981/ 25

/10/ K.Hohmuth and B.Rauschenbach, Mater. Sci. Eng. 69 /1985/ 489

/11/ K.Helmig and B.Rauschenbach, to be published

/12/ B.Rauschenbach and K.Hohmuth, phys. stat. sol. /a/ 1986, to be published

/13/ K.Hohmuth, B.Rauschenbach, A.Kolitsch and E.Richter 209/210 /1983/ 249

/14/ B.Rauschenbach and A.Kolitsch, phys. stat. sol. /a/ 80 /1983/ 211

/15/ B.Rauschenbach, A.Kolitsch and K.Hohmuth phys. stat. sol. /a/ 80 /1983/ 471

/16/ W.W. Hu, H.Herman, C.R.Clayton, J.Kozubowski, R.A.Kant, J.K.Hirvonen and R.K.McCrone, Proc. Conf. Annual Meeting Mater. Res. Soc. Cambridge /Mass./ 1979, p 92

/17/ P.D.Goode, A.T.Peacock and J.Asker, Rep. AERE-R-10696 /1982/

/18/ B.Rauschenbach and K.Hohmuth, Cryst. Res. Technol. 19 /1984/ 1425

/19/ G.Carter, Rad. Eff. Lett. 50 /1980/ 147

/20/ B.Rauschenbach and K.Hohmuth, phys. stat. sol. /a/ 75 /1983/ 159

/21/ F.P. Buncly, J. appl. Phys. 36 /1965/ 616

/22/ J.H. Ahlberg, E.N. Nilson and J.L.Walsh, The Theory of Splines and their Applications, Academic Press, New York 1967-

/23/ T.N.E. Greville, Theory and Applications of Spline Functions, Academic Press New York 1969

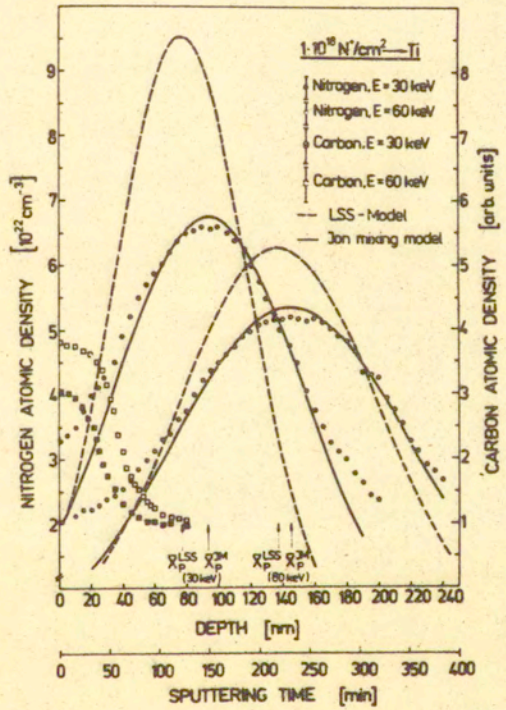

Rys.1. Concentration distribution of nitrogen and carbon after nitrogen ion implantation into titanium with an amplantation dose of 1 x 10^{18} N^+ ions/cm^2 at two energies, 30 and 60keV: •, experimental N^+, 30keV; o, experimental N^+, 60 keV, ▪, experimental, carbon 30keV, □ experimental carbon 60 keV, --- theoretical- LSS -theory —theoretical, ion beam mixing theory

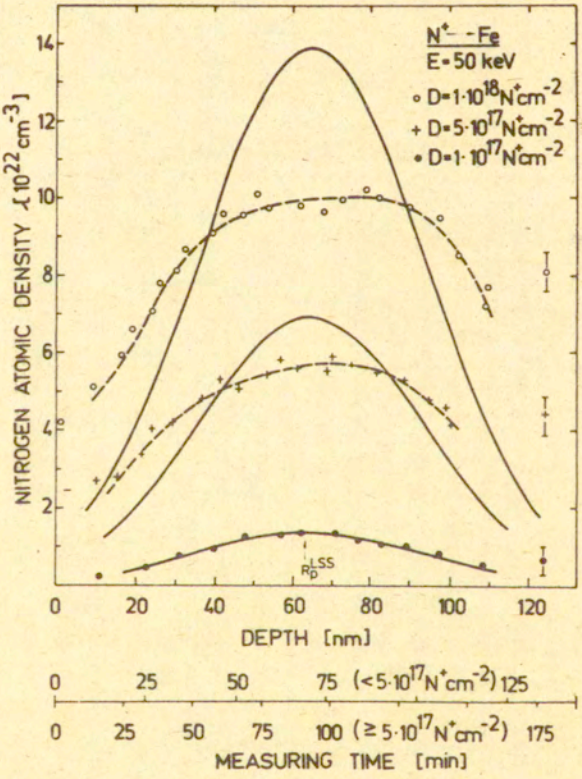

Rys. 2. Concentration profiles of implanted nitrogen in iron with 1 x 10^{17}(•) 5 x 10^{17} /+/, and 1 x 10^{18} /o/ N^+-ions/cm^2 at 50 keV. The solid curves indicate the predicted distributions according to the LSS theory

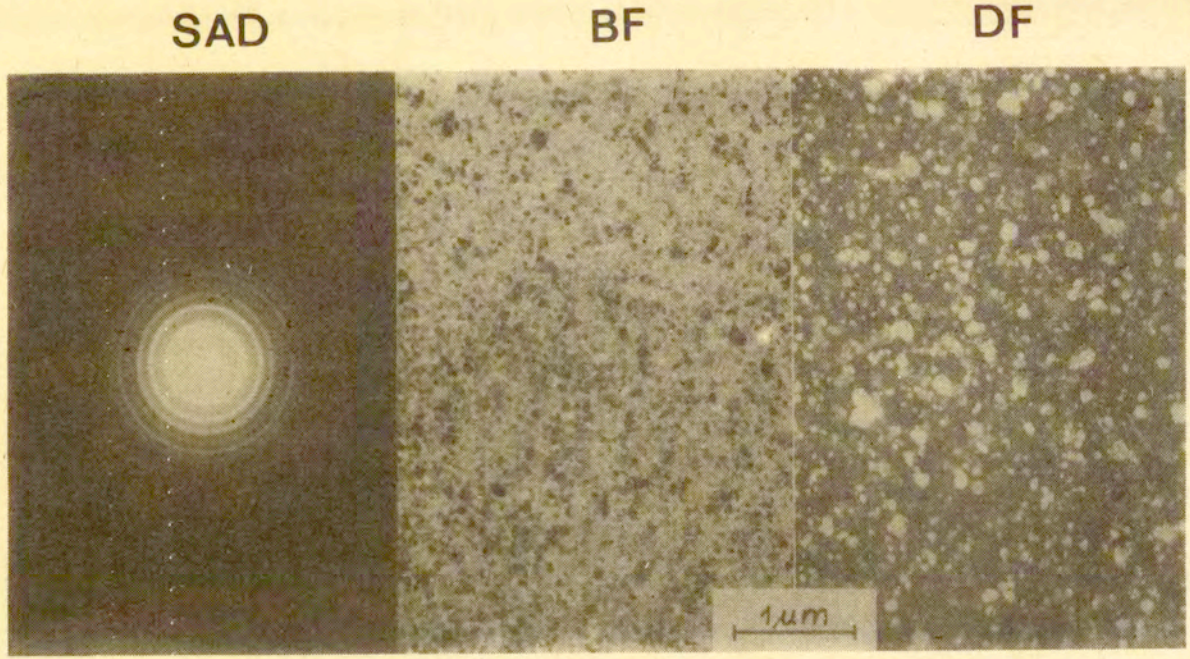

Rys. 3. Transmission electron diffraction pattern /SAD/, bright field /BF/ and dark field /DF/ micrographs of titanium implanted with 50 keV nitrogen ions to a fluence of 5×10^{17} N^+ ions/cm^2 at room temperature

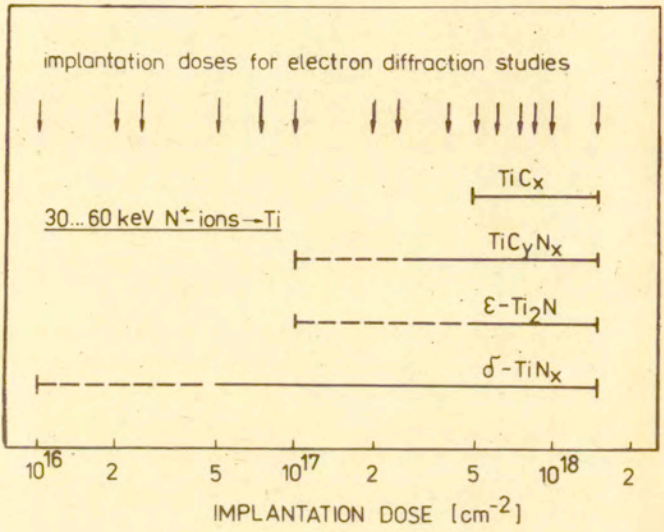

Rys. 4. Titanium nitride, titanium carbide and titanium carbonitri phases in dependence on implantation dose /state diagram/. Arrows indicate the implantation dose at which electron diffraction maesurements were made.

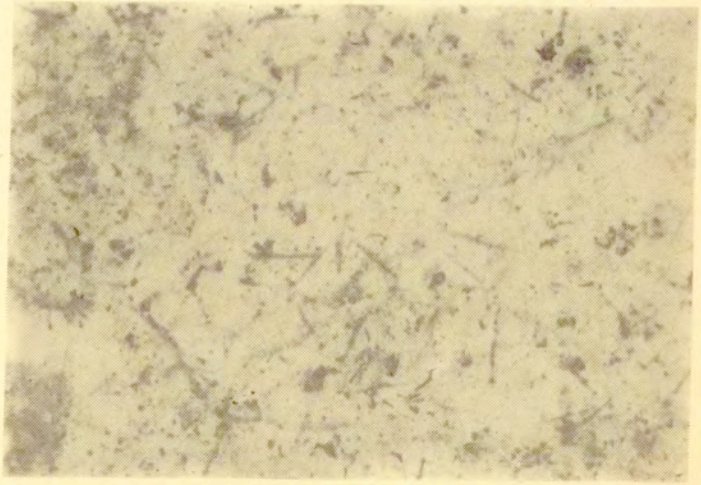

Rys. 5. HVEM micrograph of iron implanted with nitrogen ions to a fluence 5×10^{17} N$^+$-ions/cm^2

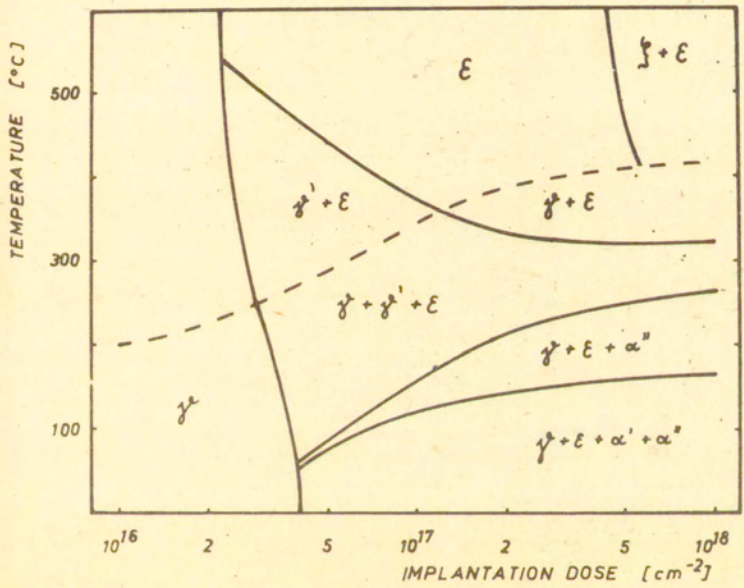

Rys. 6. Iron nitride phases in dependence on the implantation dose and temperature /state diagram/ (γ - γ austenite α' - α' -martensite, ε - ε-Fe_2N_{1-x}, α'' - α''-$Fe_{16}N_2$, γ' - γ'-Fe_4N, φ - φ-Fe_2N)

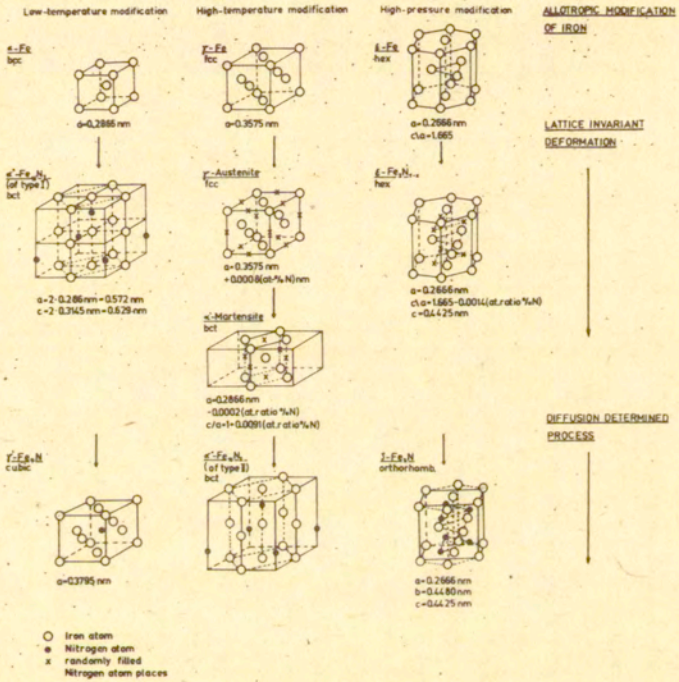

Rys. 7. Schematic diagram showing the ion implantation-induced reactions /lattice invariant deformation and diffusion determined process/ in the iron-nitrogen system / o iron atom, • nitrogen atom, x randomly filled nitrogen atom places/